

Determining sample alignment in X-ray Reflectometry using thickness and density from GaAs/AlAs multilayer certified reference materials

D Windover¹, D L Gil¹, Y Azuma², T Fujimoto²

¹ National Institute of Standards and Technology, Gaithersburg, MD 20899, USA

² National Metrology Institute of Japan, National Institute of Advanced Industrial Science and Technology, Tsukuba 305-8568, Japan

E-mail: windover@nist.gov

Abstract.

X-ray reflectometry (XRR) provides researchers and manufacturers with a non-destructive way to determine thickness, roughness, and density of thin films deposited on smooth substrates. Due to the nested nature of equations modeling this phenomenon, the inter-relation between instrument alignment and parameter estimation accuracy is somewhat opaque. In this study, we intentionally shift incident angle information from a high-quality XRR data set and refine a series of shifted data sets using an identical structural model to assess the effect this angle misalignment has on parameter estimation. We develop a series of calibration curves relating angle misalignment to variation in layer thickness and density for a multilayer GaAs/AlAs Certified Reference Material on a GaAs substrate. We then test the validity and robustness of several approaches of using known thickness and density parameters from this structure to calibrate instrument alignment. We find the highest sensitivity to, and linearity with, measurement misalignment from buried AlAs and GaAs layers, in contrast to the surface layers, which show the most variability. This is a fortuitous result, as buried AlAs and GaAs exhibit the highest long-term stability in thickness. Therefore, it is indeed possible to use reference thickness estimates to validate XRR angle alignment accuracy. Buried layer mass density information also shows promise as a robust calibration approach. This is surprising, as electron density of buried layers is both a highly-correlated phenomenon, and a subtle component within the XRR model.

PACS numbers: 61.05.cm, 68.55.jd, 06.20.fb, 07.60.Hv, 06.30.Bp

1. Introduction

X-ray Reflectivity (XRR) has been used to measure thin films since its discovery by Kiessig in 1931 [1]. Parratt in 1954 [2] developed a first-principles approach to modeling XRR data. Since that time, XRR has matured as the preferred method for non-destructive evaluation of thin film thicknesses (e.g., Lekner, [3] Chason [4], and Dalliant [5]). XRR patterns result from an interference phenomenon between layers of distinct electron density. This interference phenomenon manifests as fringes in reflected intensity as a function of the angle of incidence, θ . The ability of the method to detect interfaces non-destructively is simultaneously its strength and its weakness as a technique: layers with gradual interfaces, such as layers with inter-diffusion or high roughness, will often be difficult, if not impossible, to model. Also, because reflection takes place at glancing incidence, the technique illuminates a large sample area during measurement and averages the layer information over this area. If the sample has lateral thickness or density variation, the interference patterns will also be averaged and can potentially be washed out entirely. However, in the realm of smooth films of high lateral uniformity (e.g., optical coatings and semiconductor structures) XRR has become an invaluable tool. Both visible light characterization methods (such as optical reflectometry and ellipsometry [6]) and XRR can provide users with thickness and roughness information. However, the index of refraction of materials in the visible wavelength region often varies dramatically between materials. This introduces a high degree of uncertainty and modeling challenges with visible light characterization methods. This problem is eliminated with XRR as the index of refraction, in the hard x-ray spectrum, is near unity for all materials. Further, as the corrections due to index are negligible, XRR thickness information is easily extracted from data, making XRR an ideal approach for International System of Units (SI)-traceable measurements of thickness. For accuracy in thickness determination, we need calibration artifacts for inter-comparison measurements across XRR tools manufactured and used across the world.

In the last decade, an international collaboration under the Versailles Project on Advanced Materials and Standards (VAMAS) has performed round-robin studies on several candidate materials to be used as thickness standards for XRR [7, 8]. One structure studied by VAMAS, a three-repeat bi-layer of GaAs/AlAs (total of six layers) deposited on a GaAs wafer, was developed by the National Metrology Institute of Japan (NMIJ) as a pre-standard for a NMIJ Certified Reference Material (CRM). Data taken in 2004 by researchers at NMIJ on a similarly deposited structure, is the focus of this study. The National Institute of Standards and Technology (NIST) has been developing Bayesian approaches (see Sivia [9]) to estimate uncertainty in modeling XRR parameters [10, 11].

2. Experimental Details

XRR data are collected as a series of incident angle, θ^i , and reflected intensity, I^R , data pairs, (θ_l^i, I_l^R) stepped over N points in a range, $l = 1, 2, \dots, N$ from a starting incident angle, θ_{start}^i to ending incident angle θ_{end}^i . These data should represent the specular reflection from the surface of the sample. Specular reflection occurs when the incident and reflected angles are equal: $\theta^i = \theta^r$. Our model for XRR starts with the assumption of specular reflection. However, instrumentation effects, such as sample misalignment, δ , may cause a deviation from this condition. An XRR measurement instrument does not directly measure θ^i or θ^r . Instead, a near parallel beam of X-rays impinges on a sample which is rotated to a sample angle, ω . Intensity data is collected from a detector which is in turn rotated to a detector angle, θ^d . We define an aligned instrument (and sample) to be one where $\omega = 0$ implies that $\theta^d = 0$. Specular condition is obtained only when $\omega = \theta^i$ and $\theta^d = 2 \times \omega = \theta^i + \theta^r$; often called a $\theta - 2\theta$ scan.

The XRR data was collected on a Rigaku† ATX-G type reflectometer configured using a Cu K_α rotating anode operating at 50 kV and 300 mA with a graded parabolic multilayer mirror and a Ge (111) channel cut monochromator. This arrangement produced an intense, highly parallel X-ray source comparable to the brightest commercial XRR instruments available on the market today. Cu radiation, in laboratory settings, is the most common energy used, and provides the industry baseline for laboratory measurements using X-rays.

XRR sample alignment is difficult to perform, as it requires rocking the sample with the detector at true zero to crudely align the specimen and to set the specimen height. The sample then is rotated at a series of fixed detector angles to find the optimal omega angle for a given (trusted) detector angle. If the detector zero was incorrect, or there are any curvature effects confounding this alignment strategy, or any number of other instrument effects, then the sample and detector angles may be off by a fixed shift, and derived thickness, density, and roughness will be impacted systematically. Angular shifts in XRR intensity information have a pronounced and systematic impacts on the high frequency components of the measured data (film density and thickness). Sample height and edge effects will contribute pronounced off-specular and beam-footprint effects which cause slow varying intensity effects spread across the entire range of the data. These effects can be confounded with surface roughness and the presence or thickness of very thin surface layers.

The GaAs/AlAs multilayer structure used in this study was sample 1-08 of the BAAA4002c series provided by NMIJ (referred to here as 1-08). It was used as a pre-standard in the development of NMIJ Certified Reference Material 5201-a. The GaAs/AlAs layers were deposited using molecular beam epitaxy which produced

† Certain commercial equipment, instruments, or materials are identified in this poster to specify the experimental procedure adequately. Such identification is not intended to imply recommendation or endorsement by the National Institute of Standards and Technology, nor is it intended to imply that the materials or equipment identified are necessarily the best available for the purpose.

105 epitaxial, stoichiometric, and monotonically smooth layers, in this structure. This series
 106 of layers were provided by NMIJ to the international community for a long-term study
 107 of the stability of this structure. Based on the results of these formal and informal
 108 comparisons, NMIJ certified only the thickness of the bottom 4 layers for the final CRM
 109 as the upper 2 tended to show instability over time. Density was assumed to be near
 110 bulk values, and roughness was assumed to be interatomic-scale (0.3 nm - 0.5 nm).

111 3. Theory

112 3.1. Reflectometry modeling

113 The first-principles treatment of XRR modeling is discussed in exhaustive detail
 114 elsewhere (see [3]). However, a brief discussion of several key features of the model
 115 is useful to understand misalignment impact. XRR measurement modeling typically
 116 uses a Fresnel homogeneous layer model to treat thin films ($j = 1 \dots N$) in a stack as
 117 slabs of a fixed, refractive index, n_j . Refractive index is a complex number with a real
 118 component, δ_j , which relates to electron density and an imaginary component, β_j , which
 119 represents absorption of X-rays in a material. Refractive index is defined by convention
 120 as $n_j = 1 - \delta_j + i\beta_j$ and the δ and β values for any given element at most energies
 121 of interest in characterization are well known. Parratt developed his analysis method
 122 for XRR by solving Snell's Law of refraction for each successive layer in a stack of N
 123 layers.[2] The coefficient of reflection from any layer can be calculated by starting with
 124 the perpendicular component of the wave vector from a material layer j and by assuming
 125 a fixed n over the layer thickness:

$$126 \quad k_{zj} = k \sqrt{n_j^2 - \cos^2 \theta^i} \quad (1)$$

127 When an interface is encountered, signifying a new index of refraction n_{j+1} , we
 128 have reflection of X-rays. For the interface between the layers j and $j + 1$, we have the
 129 following Fresnel relationship, where $r_{j,j+1}$ represents the component of X-rays reflected
 130 from the $j + 1$ interface back into the j layer:

$$131 \quad r_{j,j+1} = \frac{k_{zj} - k_{zj+1}}{k_{zj} + k_{zj+1}} \quad (2)$$

132 where wave vector, $k = 2\pi/\lambda$, and λ is the X-ray wavelength.

133 Parratt's insight to this problem was to build a recursion relation for the reflection
 134 coefficient from every successive interface, j to $j + 1$ in a stack, and substitute in the
 135 reflections from lower levels of the structure, all the way to the bottom of the stack (i.e.,
 136 the substrate).

$$137 \quad X_j = e^{2ik_{zj}z_j} \frac{r_{j,j+1} + X_{j+1}}{1 + r_{j,j+1}X_{j+1}} \quad (3)$$

138 where z_j is the thickness of layer j .

139 All successive reflection coefficients from X_{j-1} to X_0 can be solved by using
 140 successive substitutions of Eqns. 2 and 3, with the special case that, since the substrate

141 is assumed to be infinite, we have no reflection from its lower interface: $X_{N,N+1} = 0$ for
 142 an N-layer stack. The measured reflection intensity is then $I^R = |X_0|^2$.

143 Layer thickness information is “locked” into the recursion though each instance
 144 of z_j , and layer density information enters as a function derived from the index of
 145 refraction, n_j , for each layer within the recursion. An XRR structural model is defined
 146 by a set of parameters for layer thickness $t_j \equiv z_j$, layer density, $\rho_j = f(n_j)$, and layer
 147 roughness, σ_j . The fundamental observation for this work is that I^R is a function of θ^i
 148 through each instance of k_{z_j} in the recursive equation. Separation of these parameters
 149 is impossible due to the nested, interdependent nature. The focus of this study will be
 150 to determine both severity and parameter refinement trends given intentional shifting
 151 of the observed θ^i for high quality data and a model test system.

152 3.2. Data refinement approach

153 Our data refinement approach follows the structure and notation of Wormington
 154 [12]. A model is developed assuming a limited number of layers and a narrow
 155 range of allowed (plausible) thickness, roughness, and density parameters which are
 156 constrained as tightly as possible by any ancillary measurements and deposition
 157 input information. For example, surface roughness can be measured by atomic
 158 force microscopy. Substrate roughness can be constrained by assuming typical wafer
 159 specifications, and cross-sectional thickness information can be constrained using
 160 transmission electron microscopy or allowed deposition times and typical deposition
 161 rates. Using this highly constrained structural model, reflection intensity values can
 162 be simulated over a range of measurable angles that mimic real measurement data,
 163 (θ_i, I_i^{R-calc}) . This simulated intensities is then compared to measured intensities, to
 164 determine the ‘goodness-of-fit’ for a given set of model parameters, \mathbf{p} , and this process
 165 can be repeated for a range of test cases, \mathbf{p} .

166 It is common to show χ^2 or goodness-of-fit (GOF) plots as a function of parameter
 167 variation to establish best fit between data and mathematical model, for example
 168 see [13]. One of Wormington’s early achievements in XRR data analysis was the
 169 implementation of alternative χ^2 strategies for fitting to data. XRR measurements often
 170 scale over many orders of magnitude requiring modification to traditional data weighting
 171 schemes. Wormington implemented several cost functions for XRR data refinement.
 172 The mean square error (MSE) of the log of reflected intensity, $\log I_R$, values provides a
 173 robust cost function for refining XRR data and where \mathbf{p} represents all the parameters
 174 used in the XRR model:

$$175 \quad MSE_{log}(\mathbf{p}) = \frac{1}{N-1} \sum_{j=1}^N [\log I_j^R - \log I_j^{R-calc}(\theta_j; \mathbf{p})]^2 \quad (4)$$

176 MSE_{log} allows for oscillation data contained several decades below the incident
 177 intensity, I_o , to still contribute to the model refinement. Figure 1 a) shows specular XRR
 178 data, with log of reflected intensity, $\log I^R$, in counts as a function of incident/reflection

179 angle θ in radians. Oscillation data is present over nearly seven orders of magnitude
 180 in intensity. Traditional χ^2 would ignore contributions from the last five orders of
 181 magnitude of the data.

182 Wormington’s other revolutionary contribution was the use of Differential Evolution
 183 (DE), a type of Genetic Algorithm (GA), to refine XRR data. The GA method tests a
 184 large population of potential parameter solutions, \mathbf{p} , simultaneously against XRR data
 185 with one of the modified cost functions, (e.g., MSE_{log}). Of this large population of
 186 solutions, only the ‘fittest’ solutions – i.e., those with the lowest MSE_{log} – are allowed
 187 to continue. These solutions are then bred or allowed to intermix parameters $p(x_j)$,
 188 and then produce a new large population of solutions for testing against the XRR
 189 data. This culling, breeding, culling model is cycled through hundreds to thousands of
 190 generations to select the global minimum solution. This refinement approach does have
 191 one implicit limitation, in that it cannot tell you directly the uncertainty of parameters
 192 within a model, but only the best set of parameters. In this study, we compare these
 193 best parameter sets, \mathbf{p} , for each misalignment and look for variational trends in our
 194 parameters. This tests the sensitivity of each parameter to angular misalignment,
 195 provided the GA was successful at finding the global minimum for the misaligned
 196 XRR data. The allowed parameter ranges in a model can sometimes influence the best
 197 solution, especially for intentionally misaligned data. Therefore, we use large ranges for
 198 parameter estimates in such a study.

199 3.3. Introduction of sample misalignment

200 To simulate misalignment of the reflectometer zero angle, we shift the angle, θ^i , by a
 201 fixed amount, δ ,

$$202 \quad \theta_j^{misalign} = (\theta_j^i + \delta),$$

203 for each angle in the initial, well-aligned dataset. We then generate simulated
 204 misaligned data which we then fit for each misalignment, $\delta = [-0.025, -0.020, -0.015,$
 205 $-0.010, -0.005, 0, 0.005, 0.010, 0.015, 0.020, 0.025]$ in $^\circ$. A typical XRR experiment will
 206 collect intensity data over an angular range of 3° . A misalignment of 0.005° corresponds
 207 to just a 1/600th shift for the total angular range of the scan and as such, may be
 208 assumed to have an insignificant effect. However, our modeling shows that even such a
 209 small misalignment can have a substantial impact on parameter estimates.

210 4. Results and Discussion

211 The initial, well-aligned XRR data-set contained 620 (θ_j, I_j^R) measurement pairs
 212 collected on a commercial XRR instrument at NMIJ using sample 1-08, covering a
 213 range of 0° to 3.1° in θ_j in 0.005° steps. Each of the 11 data sets, one aligned, and 10
 214 misaligned, was fit using a GA refinement. Each GA refinement used a population of
 215 over 200 members with random parameters, \mathbf{p} . Each GA was run for 5,000 generations
 216 and from several choices of initial parameter values in order to verify that the true global

217 minimum was found. Table 1 provides the allowed ranges for the 23 model parameters
 218 used in our refinements. Note that our prior knowledge of film thickness information
 219 was used to constrain multilayer thickness within a narrow window (1 nm for buried
 220 layers), and roughness to atomic feature scales (0.2 nm to 0.5 nm) assuming very-high
 221 quality interfaces with no interdiffusion; however, density was allowed to vary across a
 222 large range (0.5 to 2 times bulk density values). A second study was performed with a
 223 wider range of allowed roughness parameters (Table 2) to address issues in refinement
 224 of surface layers for highly misaligned XRR data. We performed GA refinement with
 225 both NIST-developed software[10, 11] and a commercial package for comparison (Bede
 226 REFS 4.5). Results from both software packages and both parameter ranges are shown.

227 Figure 1 shows: a) the original data (aligned) GA refinement, and b) the $\delta =$
 228 $+0.005^\circ$ GA refinement. In both cases, the fit (line) to the data (points) are nearly
 229 perfect, with very little to indicate either misaligned or improperly modeled information.
 230 In comparison, figure 2 shows the results of: a) $\delta = +0.025^\circ$ GA refinement and b)
 231 $\delta = -0.025^\circ$ GA refinement. In both cases, we see substantial deviations between
 232 GA (line) and data (points). Several peaks are missed entirely in both refinements,
 233 and oscillation intensities vary substantially between model and data. This will have a
 234 significant impact on the density parameter estimates for these highly misaligned cases.

235 Figure 3 shows the GOF results for the MSE_{log} GA refinements for NIST,
 236 commercial, and commercial with wide allowed roughness ranges. The better agreement
 237 between model and data from figure 1 is clearly seen by a minimum in the range of
 238 $\delta = 0$ to $+0.005^\circ$. However, we do see a systematic shift between the GOF results
 239 from using Table 1 and Table 2 (wide). Wider roughness ranges accommodated more
 240 opportunities for surface roughness to exchange with surface layer thickness and provide
 241 lower minimum GOFs for the negative offset angle, $\delta < 0$, cases. This illustrates the
 242 difficulty in using GOF as the mechanism for determining optimal alignment. Bias from
 243 allowed parameter ranges can directly affect GOF.

244 Evaluation of top layer(s) thickness as a function of δ led to uninterpretable results
 245 containing sharp discontinuities. Instead, we concentrated on layers deeper into the
 246 structure. Figure 4 shows thickness as a function of δ for the bottom four buried GaAs
 247 and AlAs layers (see Table 1 for stack numbering). All layers show a surprisingly linear
 248 relationship suggesting the utility of using a simple linear regression analysis which
 249 calculates the quality of the linearity or the coefficient of determination, R^2 , with regards
 250 to calculated thickness and misalignment. In Table 3 we show these linear regression
 251 results for all four layers. The table shows that sample 1-08 evaluated thickness and
 252 intercept show excellent agreement, indicating that the sample was extremely well-
 253 aligned. Note that the $\delta = -0.025^\circ$ was omitted in linear refinements due to non-linear
 254 behavior in some parameters. The slope term represents the change in thickness with
 255 change in δ . The negative slope indicates a decrease in thickness when data is misaligned
 256 in the $+\theta^i$ direction. The R^2 values very close to 1 give us very high confidence in
 257 linearity.

258 In figure 5, we see density as a function of δ for the same four buried layers.

259 Although all of the four layers show highly linear behavior, we see that the slopes vary
260 depending on the layer under study. There is a trend for higher sensitivity in density
261 determination with layers closer to the surface. In Table 4, we show both intercept and
262 slope and coefficient of determination for the density variation data. In this case, we
263 see several key features: First, the intercept densities from the model do not correspond
264 to densities for either bulk AlAs or GaAs. For GaAs the intercept density is higher,
265 and for AlAs the intercept is lower, than theoretical bulk values. This could either
266 indicate a bias imposed by other constraints within our structural model, incorrect
267 electron density information within our analysis (i.e., errors in δ or β), or it could tell
268 us something about thin film versus bulk density for GaAs and AlAs grown by the
269 molecular beam epitaxy. There may even be a strain component to this film versus
270 bulk density difference. All of these possible causes in difference between film and
271 bulk density represent an excellent opportunity for further study. Second, the change
272 in density with respect to misalignment angle is positive and much steeper than the
273 corresponding change in thickness. We see that density increases with increasing shifts
274 in θ^i and that density determination through XRR is highly dependent on, and sensitive
275 to, sample alignment. A small misalignment angle has a pronounced shifting effect on
276 calculated density. This may explain some of the sample-to-sample and measurement-
277 to-measurement variation in density often seen from XRR analysis. The R^2 values for
278 density slopes, which demonstrate the linearity of angle versus derived density are very
279 close to 1 (indicating nearly a straight line), except in the case of layer 7 (AlAs layer at
280 the surface of the GaAs substrate) which shows some variation from linearity.

281 The linear nature of the thickness and density with respect to δ suggests that
282 first order extrapolations could provide us with a test for systematic errors of sample
283 misalignment in commercial XRR instruments. Most XRR tools have an automated
284 alignment procedure to validate the specular nature of a measurement prior to collection.
285 Performing XRR scans with this GaAs/AlAs pre-standard (or an available multilayer
286 standard, such as the NMIJ CRM) for several sample re-mountings could establish
287 the alignment repeatability for the instrument. In this scenario, some number of data
288 sets (say 10) could be collected and analyzed with commercial GA software, and then
289 the thickness and/or density parameter estimates could be compared to the reference
290 values, to establish any systematic differences in thickness and/or in density, following
291 our determined slope relationships. As an example, Tables 3 and 4 provide a simple
292 alignment recipe for an instrument, if one has the same pre-standard sample available
293 to measure. A density for Layer 6 of 5.74g cm^{-3} would indicate a misalignment δ of
294 0.01° . If this higher density value was determined consistently over a set of 10 runs, the
295 instrument would be clearly misaligned and could be offset accordingly. This approach
296 would work on any tool, provided the same energy (Cu K_α), same angular range, and
297 same model parameter ranges (see Table 2) were used in the refinement, and that a
298 refinement software could achieve a true global minimum for each analysis. Radically
299 different beam conditioning optics may impact this type of analysis, and sample height
300 errors can also have consequences. A more rigorous study is needed to establish the

second order impacts of these additional instrumental effects.

5. Conclusions

This paper illustrates the merits of using a Certified Reference Material, in this case a multilayer AlAs/GaAs CRM from NMIJ, in the assessment of sample alignment for the X-ray Reflectometry method. Sample alignment information can be better inferred through thickness (and possibly density) variation, than through more traditional GOF minimization. Over a reasonable range of sample misalignments ($\delta \pm 0.02^\circ$), both thickness and density vary linearly for the buried layers, allowing for direct extrapolation of misalignment effects. A combined strategy of assessing both thickness and density from buried layers of the multilayer structure may yield the best alignment assessment ($U\{\delta\} < 0.005^\circ$). This combined approach needs further study, as density parameters have not been certified. Note that this technique, by its nature, relies on the availability and validity of thickness and/or density certified parameters from a traceable reference material. By comparing systematic bias in these parameters, it is possible to assess potential misalignment errors caused by mounting and stage/sample alignment approaches on a commercial reflectometer. This is very important in the field, as sample alignment is often the dominant source of uncertainty in XRR measurement for high quality films.

To date, these studies have only been developed using a single data set. Future work in this area will involve the automation of this alignment testing procedure to allow for repeatability testing of these results from multiple measurements and multiple instruments using the same specimen (CRM) to explore the limits of this approach.

References

- [1] H. Kiessig. Interferenz von röntgenstrahlen an dünnen schichten. *Ann. Phys.*, 10(5):769, 1931.
- [2] L.G. Parratt. Surface studies of solids by total reflection of x-rays. *Phys. Rev.*, 95:359, 1954.
- [3] J. Lekner. *Theory of Reflection: of Electromagnetic and Particle Waves*. Developments in Electromagnetic Theory and Applications. Martinus Nijhoff Publishers, Dordrecht, 1987.
- [4] E Chason and TM Mayer. Thin film and surface characterization by specular x-ray reflectivity. *Critical Reviews in Solid State and Materials Sciences*, 22(1):1–67, 1997. WOS:A1997WR06600001.
- [5] J. Daillant and A. Gibaud, editors. *X-ray and Neutron Reflectivity: Principles and Applications*. Springer, 1st edition, December 2010.
- [6] M. Krämer, K. Roodenko, B. Pollakowski, K. Hinrichs, J. Rappich, N. Esser, A. von Bohlen, and R. Hergenröder. Combined ellipsometry and x-ray related techniques for studies of ultrathin organic nanocomposite films. *Thin Solid Films*, 518(19):55095514, 2010.
- [7] P. Colombi, D.K. Agnihotri, V.E. Asadchikov, E. Bontempi, D.K. Bowen, C.H. Chang, LE Depero, M. Farnworth, T. Fujimoto, A. Gibaud, et al. Reproducibility in x-ray reflectometry: results from the first world-wide round-robin experiment. *Journal of Applied Crystallography*, 41(1):143152, 2008.
- [8] R.J. Matyi, L.E. Depero, E. Bontempi, P. Colombi, A. Gibaud, M. Jergel, M. Krumrey, TA Lafford, A. Lamperti, M. Meduna, et al. The international VAMAS project on x-ray reflectivity

- 342 measurements for evaluation of thin films and multilayers Preliminary results from the second
343 round-robin. *Thin Solid Films*, 516(22):79627966, 2008.
- 344 [9] D.S. Sivia. *Data Analysis: A Bayesian Tutorial*. Oxford University Press, USA, September 1996.
- 345 [10] D. Windover, D. L. Gil, J. P. Cline, A. Henins, N. Armstrong, P. Y. Hung, S. C. Song, R. Jammy,
346 and A. Diebold. NIST method for determining model-independent structural information by
347 x-ray reflectometry. *AIP Conference Proceedings*, 931(1):287–291, 2007.
- 348 [11] D Windover, N Armstrong, JP Cline, PY Hung, and A Diebold. Characterization of atomic
349 layer deposition using x-ray reflectometry. In DG Seiler, AC Diebold, R McDonald, CR Ayre,
350 RP Khosla, and EM Secula, editors, *Characterization and Metrology for Ulsi Technology 2005*,
351 volume 788, pages 161–165. Amer Inst Physics, Melville, 2005. WOS:000233588000024.
- 352 [12] M. Wormington, C. Panaccione, K. M. Matney, and D. K. Bowen. Characterization of structures
353 from x-ray scattering data using genetic algorithms. *Philosophical Transactions of the Royal
354 Society of London Series a-Mathematical Physical and Engineering Sciences*, 357(1761):2827–
355 2848, 1999.
- 356 [13] M. Kolbe, B. Beckhoff, M. Krumrey, and G. Ulm. Thickness determination for cu and
357 ni nanolayers: Comparison of completely reference-free fundamental parameter-based x-ray
358 fluorescence analysis and x-ray reflectometry RID c-8220-2011 RID g-6295-2011. *Spectrochimica
359 Acta Part B-Atomic Spectroscopy*, 60(4):505–510, April 2005. WOS:000229955200009.

Table 1. GA parameter ranges for multilayer refinement.

Layer	Material	t/nm	σ/nm	$\rho/\text{g cm}^{-3}$
1	Al ₂ O ₃	1.0-5.0	0.1-0.3	1.0-5.0
2	GaAs	6.0-11.0	0.3-0.5	2.66-7.98
3	AlAs	9.0-10.0	0.3-0.5	1.91-5.72
4	GaAs	9.0-10.0	0.3-0.5	2.66-7.98
5	AlAs	9.0-10.0	0.3-0.5	1.91-5.72
6	GaAs	9.0-10.0	0.3-0.5	2.66-7.98
7	AlAs	9.0-10.0	0.3-0.5	1.91-5.72
8	GaAs	–	0.3-0.5	5.316

Table 2. GA with wide roughness ranges for multilayer refinement.

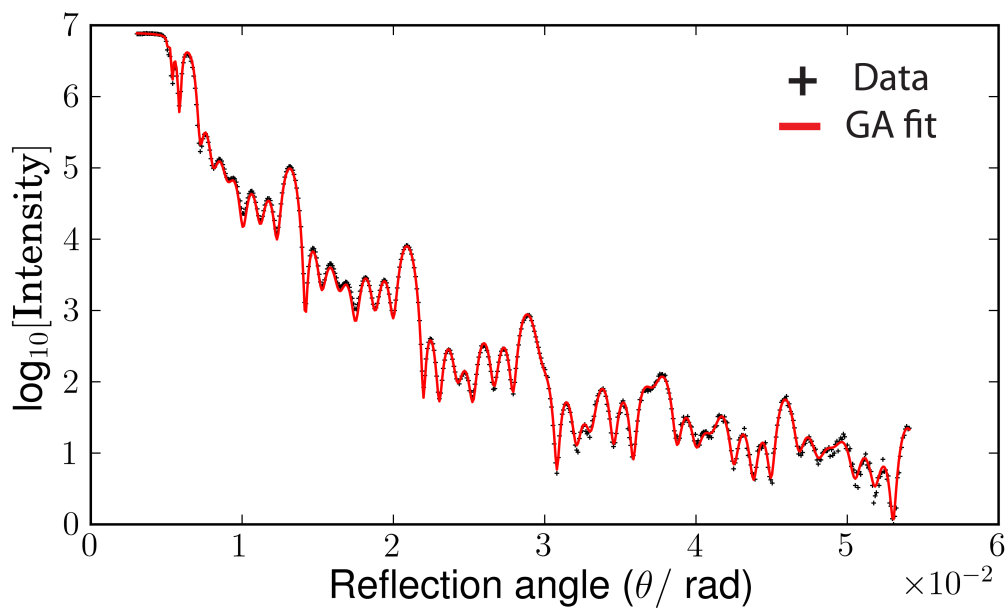
Layer	Material	t/nm	σ/nm	$\rho/\text{g cm}^{-3}$
1	Al ₂ O ₃	1.0-5.0	0.1-2.0	1.0-5.0
2	GaAs	6.0-11.0	0.1-1.0	2.66-7.98
3	AlAs	9.0-10.0	0.1-1.0	1.91-5.72
4	GaAs	9.0-10.0	0.1-1.0	2.66-7.98
5	AlAs	9.0-10.0	0.1-1.0	1.91-5.72
6	GaAs	9.0-10.0	0.1-1.0	2.66-7.98
7	AlAs	9.0-10.0	0.1-1.0	1.91-5.72
8	GaAs	–	0.1-1.0	5.316

Table 3. Linear fit to thickness in layers from misaligned data.

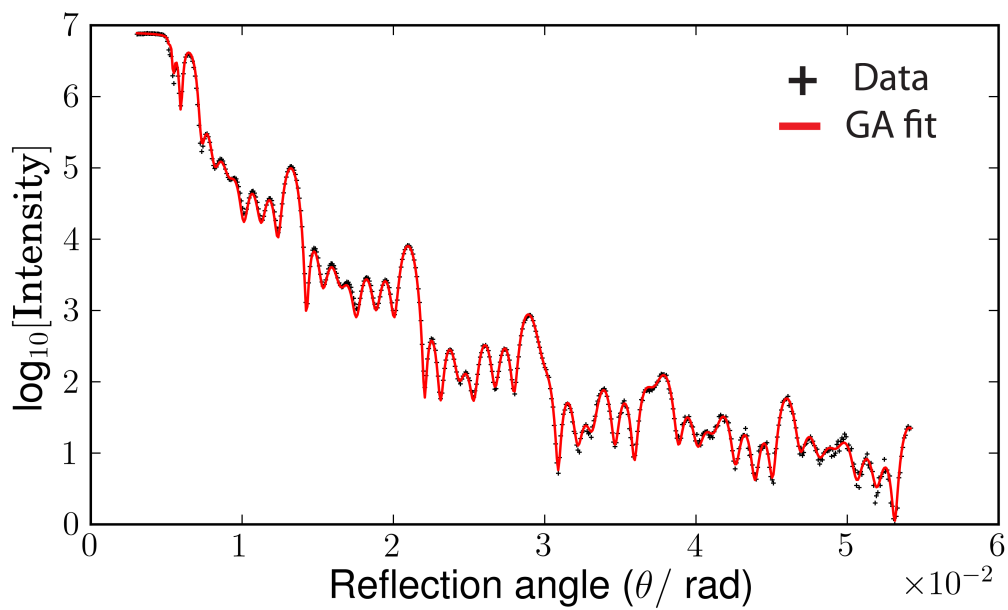
Layer	Material	Sample 1-08 t/nm	Intercept t/nm	Slope $m/$ $\text{nm } (^\circ)^{-1}$	coefficient of determination R^2
1	Al ₂ O ₃	NA			
2	GaAs	NA			
3	AlAs	NA			
4	GaAs	9.281	9.272	-2.845	0.996
5	AlAs	9.468	9.469	-4.990	0.999
6	GaAs	9.269	9.267	-3.311	0.997
7	AlAs	9.458	9.461	-5.193	0.994
8	GaAs	NA			

Table 4. Linear fit to density in layers from misaligned data.

Layer	Material	“Bulk” ρ/nm	Intercept ρ/nm	Slope $m/\text{nm } (^\circ)^{-1}$	coefficient of determination R^2
1	Al ₂ O ₃	NA			
2	GaAs	NA			
3	AlAs	NA			
4	GaAs	5.316	5.455	47.24	0.9997
5	AlAs	3.81	3.680	38.05	0.9995
6	GaAs	5.316	5.367	37.53	0.9998
7	AlAs	3.81	3.633	19.01	0.989
8	GaAs	NA			

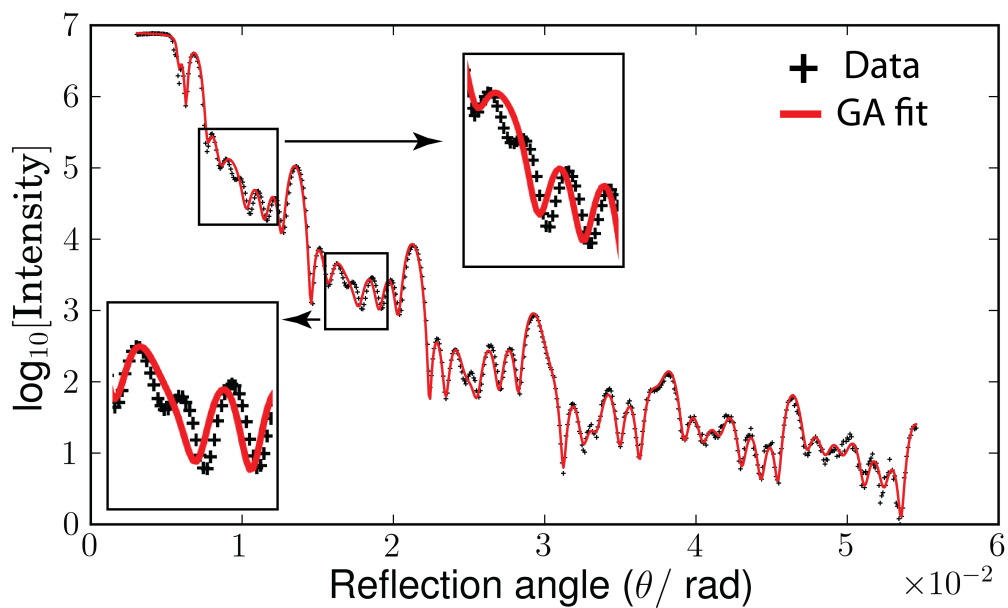


a)

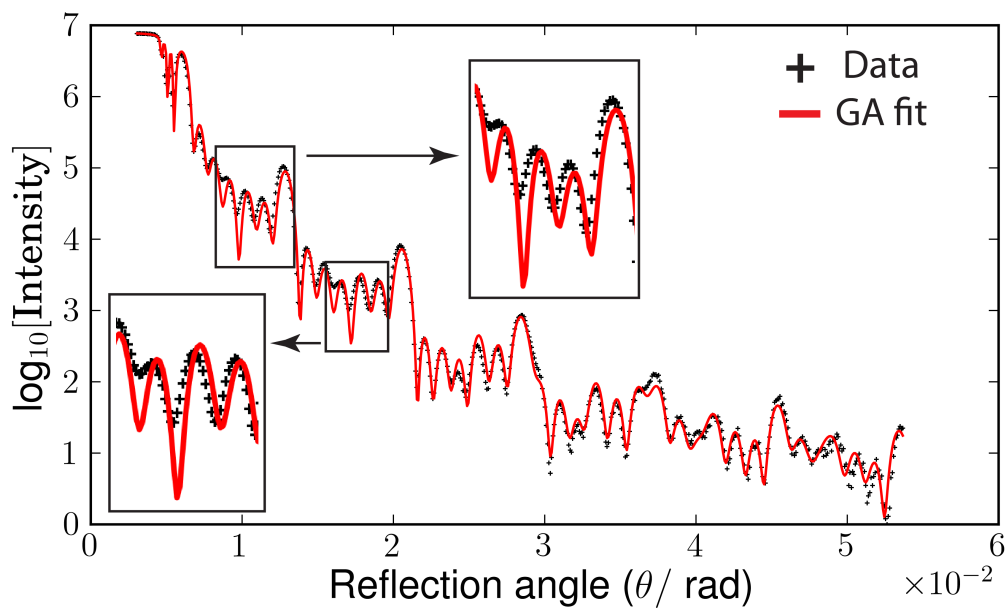


b)

Figure 1. XRR measurement data and GA model refinement result for: a) aligned data and b) data intentionally shifted $+0.005^\circ \delta$ in ω . Data is represented by points with a line representing GA refinement.



a)



b)

Figure 2. XRR measurement data and GA model refinement result for data intentionally shifted: a) $+0.025^\circ$ and b) -0.025° δ in ω . Data is represented by points with a line representing GA refinement. Inset boxes are magnified views of two regions, showing deviations between refinement and data.

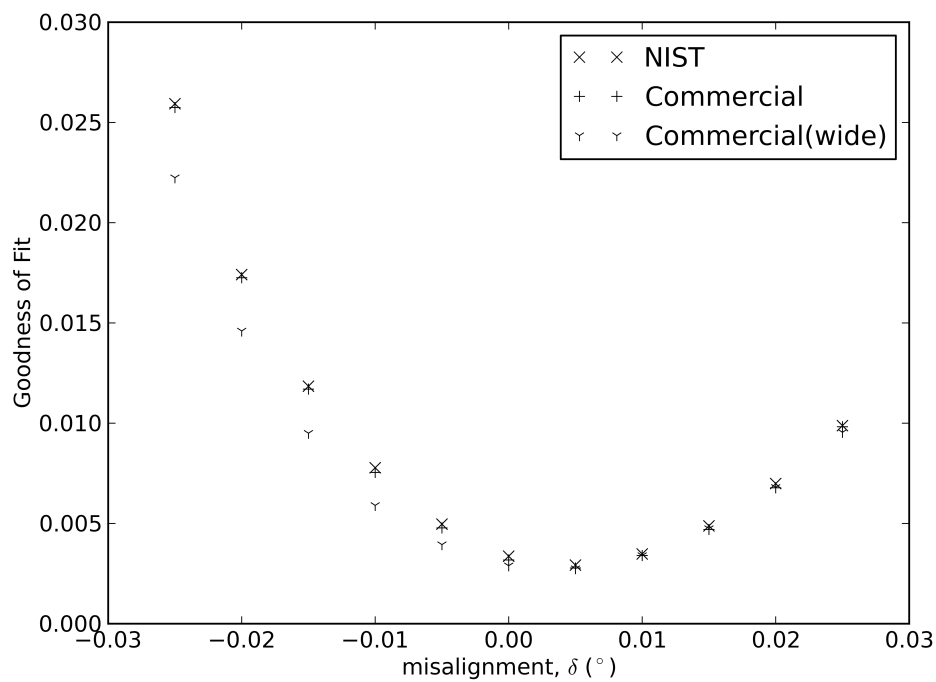
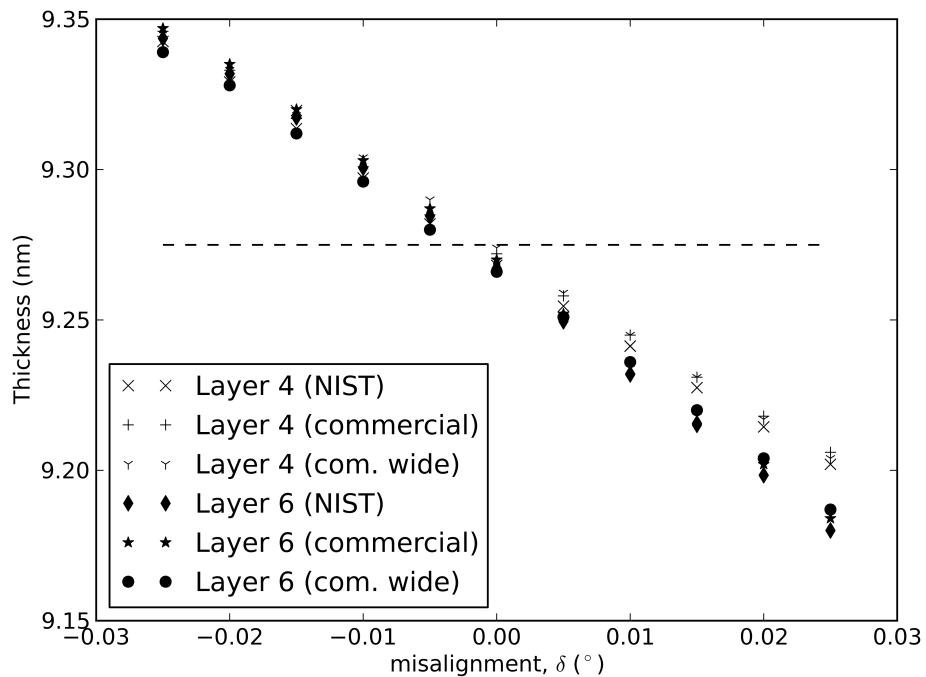
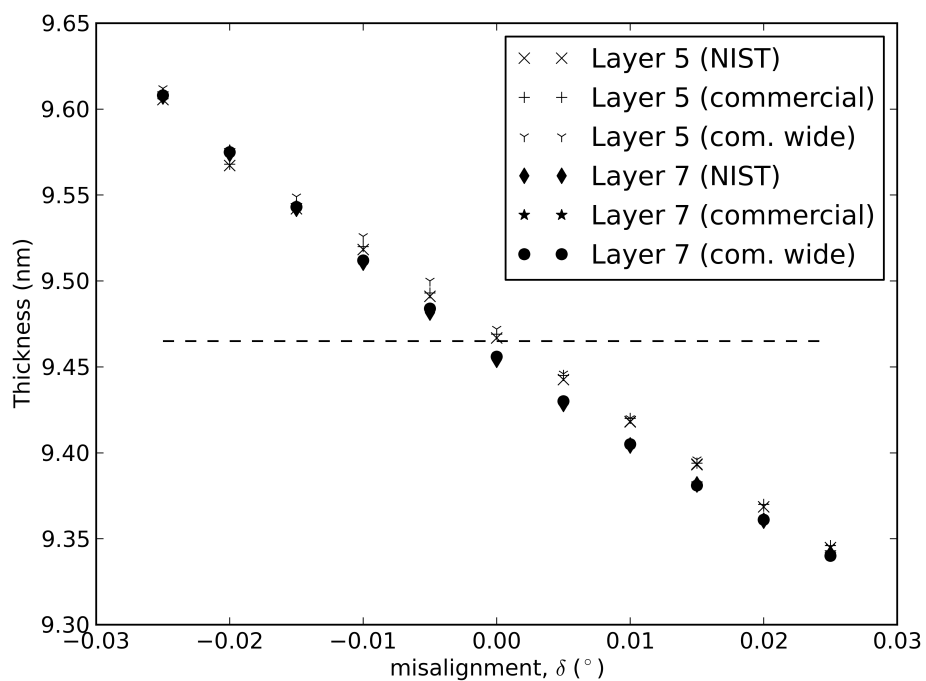


Figure 3. Goodness-of-fit for the GA refinement of the XRR multilayer model as a function of sample misalignment, δ . NIST developed XRR code is represented by x. A commercial GA XRR code is shown for comparison with + symbols.

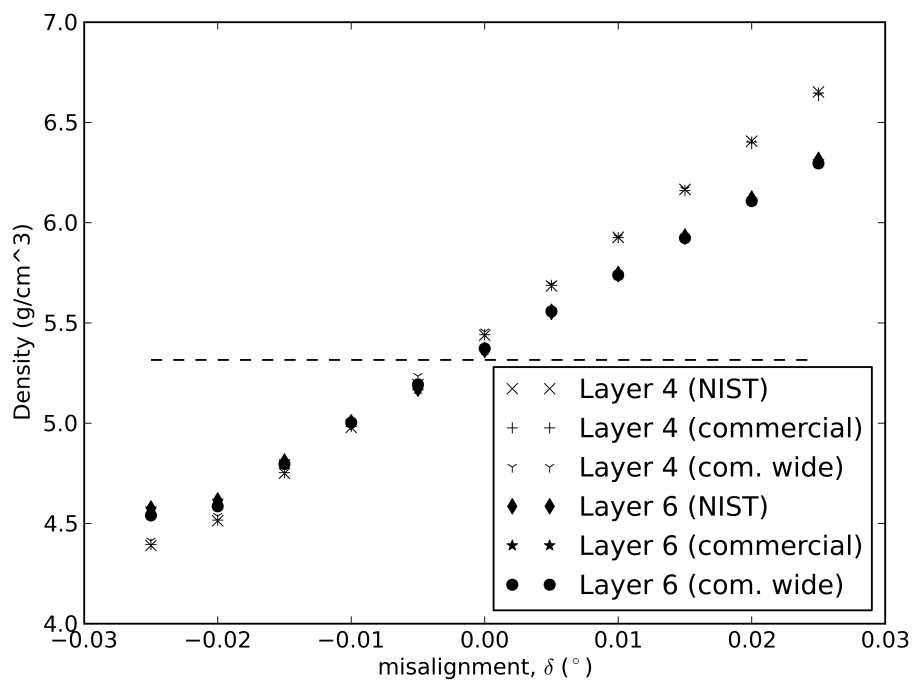


a)

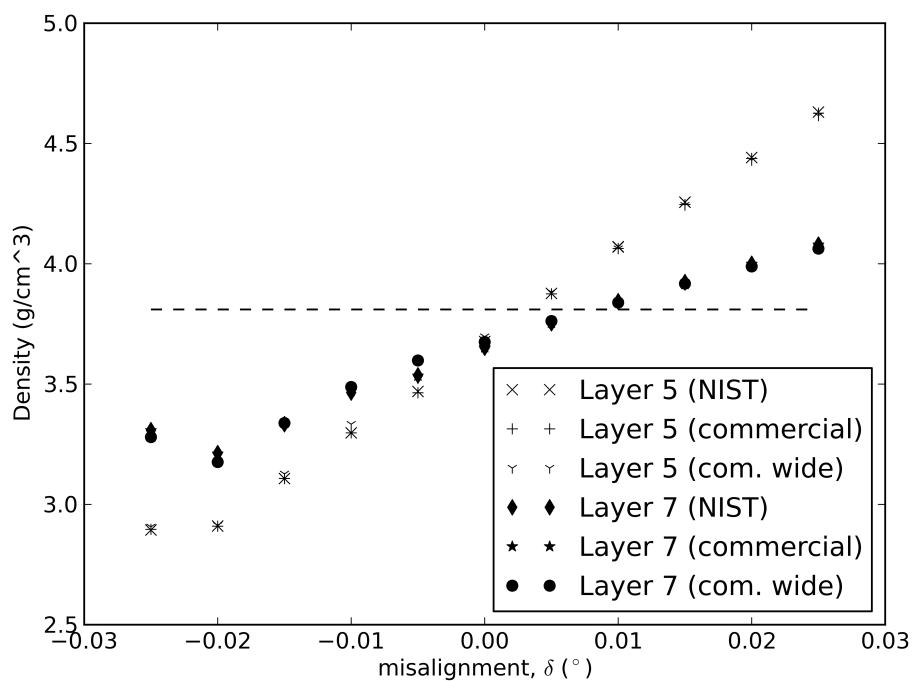


b)

Figure 4. Thickness determination of: a) GaAs layers, and b) AlAs layers, in multilayer stack, as a function of sample misalignment, δ . Note a decrease in slope for thickness as a function of sample misalignment. Dashed line represents the CRM thickness.



a)



b)

Figure 5. Density determination via genetic algorithm of: a) GaAs layers, and b) AlAs layers, in multilayer stack, as a function of sample misalignment, δ . Note the variation in the slope of density variance between layers in the stack. Layers 4 and 5 show larger slopes (more sensitivity to misalignment).